Control Science and Engineering
2018; 2(1): 36-49
http://www.sciencepublishinggroup.com/j/cse
doi: 10.11648/j.cse.20180201.14

Synthesis of a Digital Corrector for Frequency Control in Hydroelectric Power Plants

Korassaï[1, *], Yeremou Tamtsia Aurelien[2], Haman-Djalo[1], Samba Aimé Hervé[2], Ngaleu Gildas Martial[2]

[1]Faculty of Science, University of Ngaoundere, Ngaoundere, Cameroon

[2]Faculty of Industrial Engineering, University of Douala, Douala, Cameroon

Email address:

korassaipaul@gmail.com (Korassaï), ayeremou@yahoo.fr (Y. T. Aurelien), haman_djalo@yahoo.com (Haman-Djalo), aimehervesamba@yahoo.fr (S. A. Hervé), gmngaleu@yahoo.fr (N. G. Martial)

[*]Corresponding author

To cite this article:

Korassaï, Yeremou Tamtsia Aurelien, Haman-Djalo, Samba Aimé Hervé, Ngaleu Gildas Martial. Synthesis of a Digital Corrector for Frequency Control in Hydroelectric Power Plants. *Control Science and Engineering*. Vol. 2, No. 1, 2018, pp. 36-49.
doi: 10.11648/j.cse.20180201.14

Received: November 26, 2018; **Accepted**: December 17, 2018; **Published**: January 22, 2019

Abstract: The safety and reliability of an electricity grid is defined by the quality of the power supplied to consumers. One of the important criteria for the stability of electrical networks is the frequency of the voltage produced. The aim of this paper is to develop digital corrector applied to the speed control system correcting on turbines to resolve the frequency variations problems in the output of the alternator caused by the imbalance between the active power produced by the turbo-generator and the power required by the load connected to the grid in the hydroelectric plants. First, a modeling of the turbine, the servo valve - servomotor assembly, the valve - flow function, the power chain as well as the alternator of the power station is presented. Then, three controllers (Proportional–Integral–Derivative, Internal Model Control and Robust Structure Theory) are studied, simulated and their performances were tested and compared in terms of instruction tracking and robustness. The simulations were realized by MATLAB/Simulink software. For the hydroelectric power plant studied, the RST controller has the best performance.

Keywords: Turbo-Generator Group, Corrector, Frequency, Electrical Network, Regulation, Hydroelectric Plants

1. Introduction

The quality and availability of electrical energy has become a social and economic issue. The main difficulty in the distribution of electrical energy comes from the inability to store this energy in large quantities [1]. It is therefore necessary to constantly adjust producing to consumption. Motivated by the desire to reduce the fluctuations and frequency deviations caused by the imbalance between the active power required by the turbo-alternator and the power required by the load connected to the grid, many studies have been conducted on the automatic controllers during last decades [2-6].

For a long time, many advanced command synthesis methods such as Linear Quadratic Gaussian (LQG), optimal synthesis, robust Infinite H controller and Q-parameterization have been developed for such a system [7-8]. However, these methods are still insufficiently or not used in industry [9]. It is therefore necessary to make the advanced methods of the automatic more accessible to industrial users.

In this paper, the new types of optimal (PID), Internal Model Control (IMC), and Robust Structure Theory (RST) was developed, digital controller to be implemented to increase the efficiency of the frequency control system in hydroelectric power plants.

The main contributions of this work are:

a. The modeling of the turbines speed regulation chain (case of the Songloulou-Cameroon power station);
b. The modeling of the power chain;
c. The synthesis of an optimal digital PID controller;
d. Implementation of digital RST and IMC controller;
e. The realization of a virtual test bench for turbine and generator control.

In this context, the three types of correctors developed (the

optimal PID controller, the IMC controller and the RST controller) on the model of the Songloulou hydroelectric power station in order to evaluate their performances was simulated.

This paper is organized as follows: The modeling of the turbine speed control chain (case of the Songloulou-Cameroon power plant) and the power chain modeling are presented in Section 2; Section 3 presents the synthesis and optimization of the digital PID controller used in the hydroelectric plants. Section 4 presents the implementation of new types of correctors, namely the RST controller and the IMC controller. Case studies and simulation results are discussed in Section 5. Section 6 presents a virtual test bench for turbine and alternator control developed on the Laboratory Virtual Instrument Engineering WorkBench (LabVIEW) software platform. Conclusion is summarized in Section 7.

2. Modeling

The block diagram of a hydroelectric plant including the speed control system is shown in Figure 1 below, [10-11]:

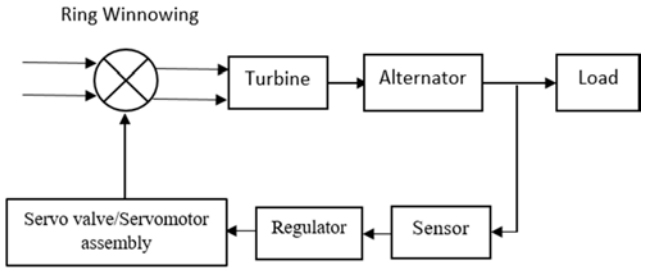

Figure 1. *Block diagram of the speed control system for a hydroelectric power plant.*

The Songloulou hydropower plant has the following characteristics: Francis Turbine (P=49.5MW, D=4.55m), synchronous alternator (S = 57MVA, Cos (φ) = 0.85, U = 10.3kV, D = 9.20m, J = 8800 t / m2), MIPREG controller 600c.

2.1. Modeling of Turbine

From the representations of [10] and [11], it will then give the reduced Bond graph representation of a Francis turbine shown in Figure 2.

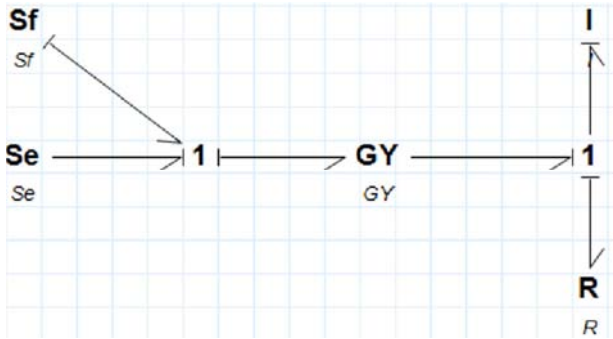

Figure 2. *Bond Graph of the Turbine.*

Where: Sf represents the flow source (flow of water entering the turbine); Se represents the source of effort (inlet pressure of the water in the turbine); I represent the inertia of the turbine.

The ratio r of the gyrator (GY) is defined by:

$$r = a\omega + b\varphi \quad (1)$$

Where ω is the rotational speed of the turbine in rad/s and φ the flow rate of water entering the turbine in m^3/s, a and b are constants that depend on the geometry of the turbine [12]. Using the cause-and-effect relationships of the gyrator element, the Euler theory applied to turbomachines [13], and the dimensional equations, is given by:

$$a = \rho \times r_2^2 \text{ and } b = \frac{\varphi}{r_1} \quad (2)$$

Where r_1 is the radius of the wheel at the inlet of the turbine in m and r_2 the radius of the wheel at the outlet of the turbine in m. By replacing the values of Sf, Se, GY, I and R, it obtain the transfer function of the turbine:

$$G_T(p) = \frac{0.663}{1+42.55p} \quad (3)$$

2.2. Modeling of the Servo Valve

The modeling of the servo valve with three amplification stages as defined in [14] allows with the parameters of the control unit to obtain the following transfer function:

$$G_s(p) = \frac{20}{1+0.645p+0.00645p^2} \quad (4)$$

2.3. Modeling the Winnowing/Flow Function

The correspondence between the winnowing (v) and the turbine water flow (d) can be deduced from the data of [15] and represented by:

$$d = 1.7967v + 0.9874 \quad (5)$$

2.4. Modeling of the Power Chain

From the charts given in [16], it is giving by:

$$Q = 16 + 90\frac{P}{H_b} \quad (6)$$

$$P = \frac{1}{90}(Q - 16)H_b \quad (7)$$

Where Q is the turbine water flow in m^3/s, P is the power available at the end of the rotor shaft in MW, H_b is the gross head of height in m. From equations (6) and (7), it obtain the Matlab/Simulink model corresponding to figure10. P_r represents the power of the load in Watts; C_r the Resistant Torque due to the load in N.m; P_m the active power produced in Watts; C_m the Motor Torque ω_{mes} the Speed measured at the rad/s and $d\omega$ the disturbance.

3. Synthesis of the PID Controller

The identification method used for the synthesis of the

digital PID controller is the empirical method of identifying Takahashi [16]. According to the data collected at the Songloulou hydroelectric plant, by open-loop tests on the process, it can be obtained with a sampling period T_e=1s the transfer function of the following PID controller:

$$C(z) = \frac{3.357z^2 - 4.657z + 1.857}{z^2 - z} \quad (8)$$

4. Contribution

4.1. Optimization of the PID Controller

The graph in Figure 3 below presents the system index responses for the PID of equation (9) and PID modified.

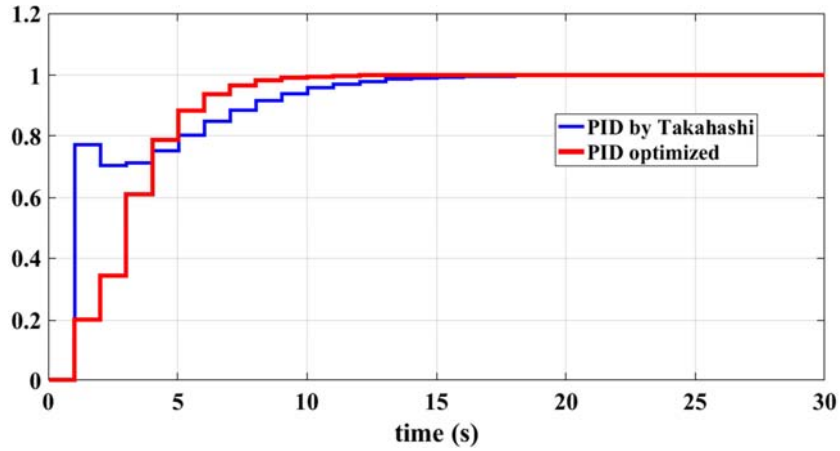

Figure 3. *Calculated PID and Modified PID Index Responses.*

The transfer function of the PID controller obtained after the optimization under Matlab is written as follow:

$$C(z) = \frac{0.25z^2 + 0.0029z + 0.2316}{z^2 - 0.88z - 0.12} \quad (9)$$

4.2. Synthesis of the Internal Model Control (IMC)

The control strategy by the internal model control is shown in Figure 4 [17].

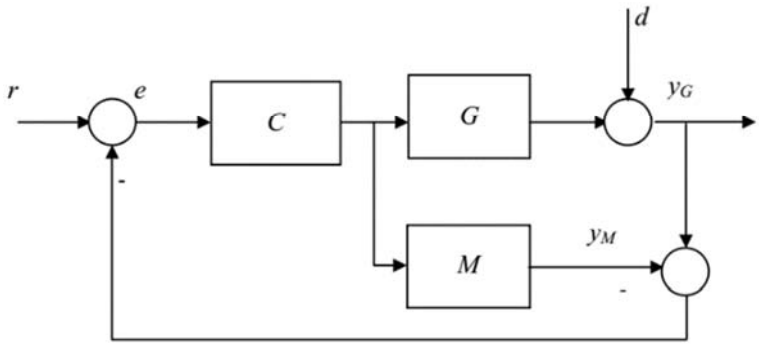

Figure 4. *Structure of the IMC Command.*

It incorporates a simulation of the process by a model M in discrete time and in state representation [17]. The command from the corrector C is applied simultaneously to the method G and its model. The output of the method and the set point are respectively denoted y_G and r; d is an additive disturbance at the output of the process.

The study of the structure allows to establish the following operating equation, linking the output Y to the input r and the disturbance d:

$$Y = \frac{CG}{1 + C(G - M)} r + \frac{1 - CM}{1 + C(G - M)} d \quad (10)$$

4.2.1. Choice of the System Model

The model of the Songloulou hydroelectric plant as established in Section 2 is represented by the following transfer function:

$$M(s) = \frac{0.0158s^2 + 1.581s + 91.62}{s^3 + 100s^2 + 157.3s + 3.643} \quad (11)$$

The index response of the system is priori quite close to a first-order system (Figure 5), so we choose a first-order model of the form:

$$M(s) = \frac{k}{1 + \tau s} \quad (12)$$

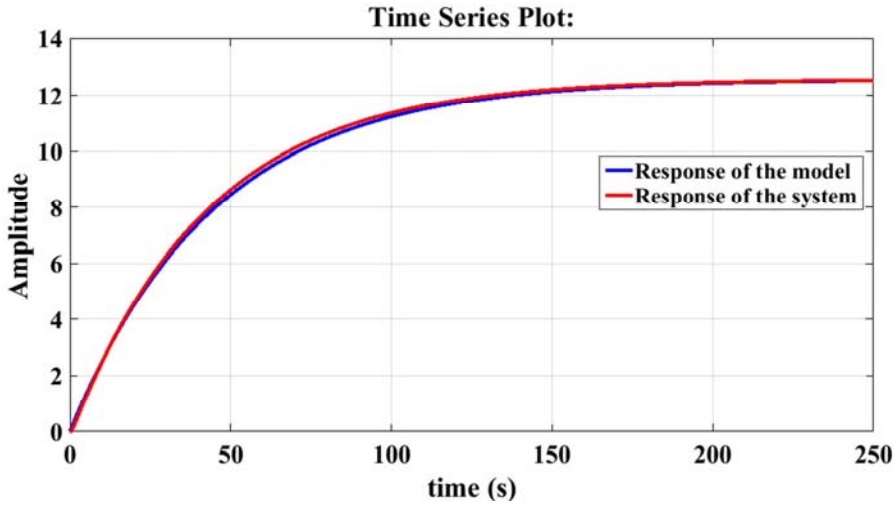

Figure 5. *Index Responses of the Systems and the Model.*

Where k is the static gain and τ is the constant time. The parameters of this model are obtained by parametric identification [16]. We get the following transfer function:

$$M(s) = \frac{25.13}{1+44.8s} \quad (13)$$

To improve the order speed without degrading the system performance, a model faster than the process was chosen.

$$\begin{cases} M'(s) = \frac{k}{1+\tau' s} \\ \tau' = \tau/4 \end{cases} \quad (14)$$

$$M'(s) = \frac{25.13}{1+10.7s} \quad (15)$$

The transfer function of the discrete model is obtained with T_e =1s:

$$M(z) = \frac{2.242}{z-0.9108} \quad (16)$$

The state representation of the dynamic system is described by the following state equations:

$$\begin{cases} x(k+1) = Ax(k) + Bu(k) \\ y_M(k) = Cx(k) \end{cases} \quad (17)$$

Where

$$A = [0.9108];\ B = [2];\ C = [1.1211]$$

Figure 6 show the discrete model in state representation.

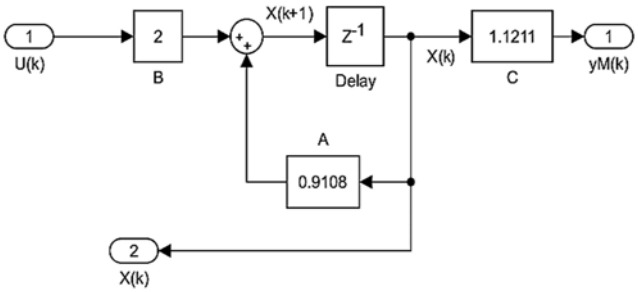

Figure 6. *Discrete Model in State Representation.*

If the corrector C is the exact inverse of the model M, then the output of the model is equal to the modified set point e [16]. From the relation giving the entry e at the instant $k + \delta + 1$ as a function of the command u at the instant k:

$$e(k + \delta + 1) = CA^{\delta+1}x(k)CA^{\delta}Bu(k) \quad (18)$$

With δ the characteristic number of the model. This relationship then expresses the law of following status feedback command:

$$u(k) = [CA^{\delta}B]^{-1}[e(k+\delta+1) - CA^{\delta+1}x(k)] \quad (19)$$

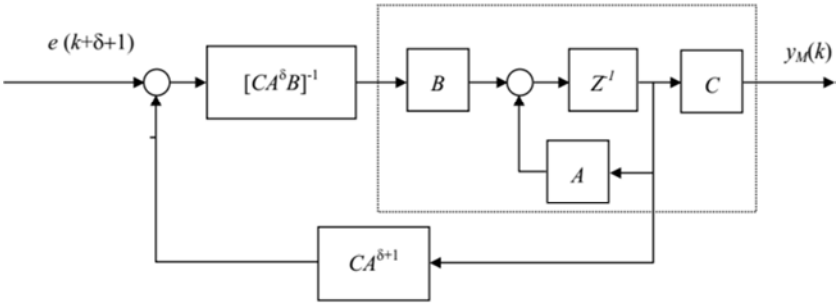

Figure 7. *State Feedback on the Model.*

This law of control poses two problems; one relates to its physical realism and the other relates to the stability of the corrector [17]. These problems are solved thanks to the introduction of an appropriate finite impulse response filter which has the task of inverting the model without taking into account its delay, in order to obtain a physically feasible transfer. And the partial inversion of the model taking into account the instability of the zeros in the prediction relation to try to compensate the fact of not being able to reverse the delay of the model [17].

Figure 8 shows the new shape of the IMC structure.

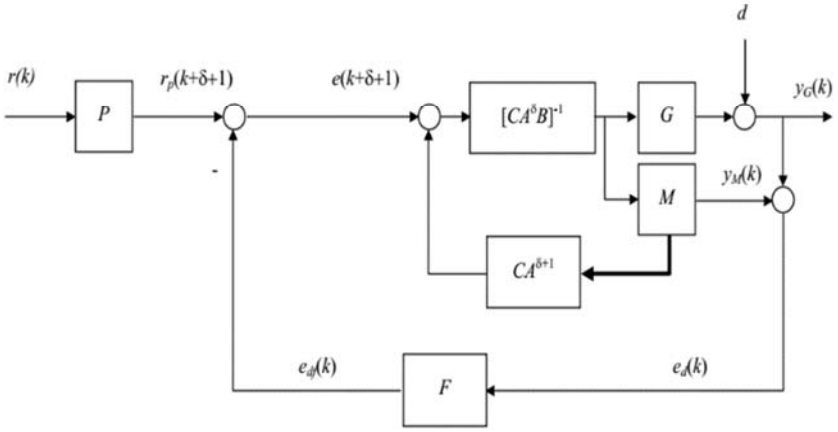

Figure 8. *Deviation and Setpoint Prediction Model.*

4.2.2. Determination of Set Point Predictor

In the approach proposed to react to the problem of system stability, the concerned with predicting the deviation signal, taking care to preserve the stability of the system despite the mismatch of the model. The characteristic number of this model is δ = 0, the set point predictor P(z) must then satisfy the following criterion [17]:

$$\begin{cases} \lim_{z\to 1}(z-1)[1-z^{-(\delta+1)}P(z)]e(z)=0 \\ P(z)=a_0 \\ e(z)=\frac{1}{(z-1)} \end{cases} \quad (20)$$

Given by:

$$P(z)=1 \quad (21)$$

And

$$e_p(k)=e(k) \quad (22)$$

To work around the problem of the stability of the corrector, it is proposed to incorporate the unstable zeros of M in the synthesis of the finite impulse response (FIR) filter, predictor of the deviation in order to ensure that the output of the model asymptotically follows the predicted input [17]. The FIR filter must then check the following relation [17]:

$$\begin{cases} \lim_{z\to 1}(z-1)[1-z^{-(\delta+1)}F(z)]e(z)=0 \\ F(z)=\frac{h_0(\alpha)-h_1(\alpha)z^{-1}}{1-\alpha z^{-1}} \\ e(z)=\frac{1}{(z-1)} \end{cases} \quad (23)$$

The parameter α is used to control the dynamics of the filtering. In order to ensure the stability of this filter and to keep it a physical sense, α must satisfy 0 <α< 1.

For $\alpha = 0.2$; given by:

$$F(z)=\frac{1.42-0.59z^{-1}}{1-0.16z^{-1}} \quad (24)$$

4.3. Implantation of the RST Controller

A system controlled by an RST regulator has the structure defined in Figure 9 [18].

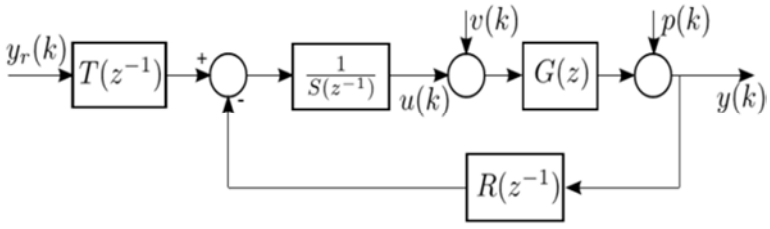

Figure 9. *Structure of the RST Command.*

The intent is to determine the polynomials R (z^{-1}), T (z^{-1}), S (z^{-1}) knowing that it is desired that the transfer function in regulation and closed loop is of the form [18-19]:

$$G(z^{-1})=\frac{Y(z)}{U(z)}=\frac{z^{-d}B(z^{-1})}{A(z^{-1})} \quad (25)$$

With $d \geq 1$ the number of complete sampling periods contained in the pure delay z^{-1}.

The sampled model of the corresponding system with the sampling period $T_e = 1s$ and a blocker of order 0 (BOZ) is:

$$G(z^{-1}) = \frac{z^{-1}(0.2943+0.1691z^{-1}+1.921e-05z^{-2})}{1-1.184z^{-1}+0.2023z^{-2}} \quad (26)$$

$$G(z^{-1}) = \frac{z^{-d}B^{+}(z^{-1})B^{-}(z^{-1})}{A^{+}(z^{-1})A^{-}(z^{-1})} \quad (27)$$

$$A(z^{-1}) = (1 - 0.9768z^{-1})(1 - 0.2071z^{-1}) \quad (28)$$

$$B(z^{-1}) = (1 + 0.5744z^{-1})(1 - 0.00011z^{-1}) \quad (29)$$

No zeros and poles of the system to be regulated must be compensated for this synthesis:

$$B^{+}(z^{-1}) = 1 \quad (30)$$

$$B^{-}(z^{-1}) = 0.29429z^{-1}(10.5744z^{-1})(10.00z^{-1}) \quad (31)$$

$$A^{+}(z^{-1}) = 1 \quad (32)$$

$$A^{-}(z^{-1}) = (1 - 0.9768z^{-1})(102071z^{-1}) \quad (33)$$

The performance in regulation is specified by the closed-loop model [19]:

$$H_m(z^{-1}) = \frac{z^{-d}B_m(z^{-1})}{A_m(z^{-1})} \quad (34)$$

The following closed loop set point tracking model is defined:

$$H_m(z^{-1}) = \frac{0.8781z^{-1}}{1-0.08698z^{-1}} \quad (35)$$

The performance in setpoint tracking is such that one can follow a constant setpoint without error.

$$H_m(1) = 1 \quad (36)$$

The polynomial $R'(z^{-1})$ and $S'(z^{-1})$ are obtained by solving the Diophantine equation:

$$A^{-}(z^{-1}).(1 - z^{-1}).S'_1(z^{-1}) + B^{-}(z^{-1})R'(z^{-1}) = A_0(z^{-1}).A_m(z^{-1}) \quad (37)$$

The polynomials $S(z^{-1}), R(z^{-1})$ and $T(z^{-1})$ are generally given by [19]:

$$\begin{cases} S(z^{-1}) = B^{+}(z^{-1}).S'(z^{-1}) \\ R(z^{-1}) = A^{+}(z^{-1}).R'(z^{-1}) \\ T(z^{-1}) = B'_m(z^{-1}).A_0(z^{-1}) \end{cases} \quad (38)$$

With:

$$\begin{cases} S'(z^{-1}) = (1 - z^{-1})S'_1(z^{-1}) \\ B_m(z^{-1}) = B^{-}(z^{-1}).B'_m(z^{-1}) \\ A_0(z^{-1}) = 1 \end{cases} \quad (39)$$

Following transfer functions was obtained:

$$R(z) = \frac{3.0006z^2-32354z+0.5157}{z^2} \quad (40)$$

$$S(z) = \frac{1-0.5689z^{-1}-0.4311z^{-2}}{z^3} \quad (41)$$

$$T(z^{-1}) = 0.2810 \quad (42)$$

5. Results and Discussions

The response of the system to a load disturbance (demand of 48 MW power) appearing at 500s, under a gross drop height of 39m in the presence of PID controller (Figure 10), IMC (Figure 11) and RST (Figure 12) was simulated note that during a sudden change in the power absorbed by the network (Figure 17), the speed of movement of the turbine needle saturates, which inevitably leads to a large exceeding of the output frequency of the turbine alternator (Figure 16).

Depending on the difference between the output frequency of the alternator and the set value, the corrector reads the numerical value of the error every Te (Te = 1s), stores it in memory and from an algorithm, produces a digital control signal to impose a current to the servo valve, which will allow a corresponding adjustment oil pressure. The curves of Figures 13 show the flexibility of the various correctors with respect to the constraints of the mechanical members. We note that the control current produced in the presence of the PID corrector (in green) increases slightly every Te seconds and stabilizes at the value of 3.5 mA; the digital control signal produced by the corrector IMC at time T*e* acts on the output only from the instant 2Te, which justifies the variation of the current of command every 2 seconds (in red). The current produced in the presence of the RST controller increases until reaching the value of 2.74mA at t = 501s increases and stabilizes at the value of 3.5mA, the more the system evolves towards the setpoint plus the difference between the output and the instruction decreases what justifies the evolution of the current. This evolution of the control current at each sampling period will cause a moderate variation of the winnowing (Figure 14), that is to say the opening of the water propagation guidelines on the blades of the turbine which in turn will cause an increase in the flow rate of turbined water (Figure 15) necessary to reduce the speed of the turbine to a value that can eliminate the difference found at the output of the alternator. Figure 19 shows the load torque and the motor torque. The analysis of the curves in Figure 16 allows us to draw up the table below.

Table 1. *Comparison of Setup Times to 4% and Maximum Overrun According to Different Markers.*

Controller	Response time at 5% (s)	Overshoot (Hz)
PID	72	5.53
IMC	6.7	3.7
RST	0	1.75

The actual operating conditions was introduced, the nominal load is 48MW and white Gaussian noise (Figure 18). It can be seen that despite the disturbances, the frequencies (Figure 18) remain within the recommended operating range ([48Hz-52Hz]).

The simulation results are recapitulated in table 2. This

table presents the data collected by simulation of the model of the hydroelectric power plant. A comparative study of the corrected frequencies, water flows rate, winnowing, control currents of the servovalve, motor torques and powers produced by the turboalternator group for the various types of correctors proposed after the appearance of the load disturbance (demand of 48MW power) were made in this table. It is noticed that after 2s only the system controlled by corrector RST reacts and the trajectory of the frequency returned back to the normal range ([48-52] Hz) with a water flow of $53{,}81m^3/s$, a motor torque of 13,49 Nm and a power produced of 18MW and is stabilized definitively in the interval tolerated after 13s. The response time which we raised for corrector IMC is 6,7s with a water flow rate of $41{,}22\mathrm{m}^3/\mathrm{s}$, frequency of 48,28Hz and power produced of $18{,}50\mathrm{MW}$.

Indeed, the frequency of the network is brought back to its reference value with $50\mathrm{Hz}$ for a speed of the turbine of $12{,}56rad/s$ completely identical to that envisaged under nominal operation by the manufacturer. The other parameters such as the control current of the servovalve, the water flow rate entering the turbine, winnowing, thus its speed of the turbine as we had already specified remain during their evolution in the intervals of safety and optima effectiveness and all the constraints related to the regulation organ (servovalve) are respected.

The simulation results clearly show that the set-point tracking and disturbance rejection are achieved and it offers robustness. From the analysis of Table 2 it follows that the system control effect is satisfactory without overshoot, static error and the system has good traceability. The resulting outputs responses of the system are in order affirm the effectiveness of the proposed internal model controller (IMC) and RST controller, the desired tracking behavior (following the reference) is obtained independently of the desired regulation behavior (rejection of a disturbance). The RST control is evaluated by the tracking and Regulation with Independent Objectives. This method provides a good tracking of the reference: no lagging error and no overshoot.

6. Virtual Instrumentation Test Bench for Turbine and Alternator Control

The graphical interface of the simulator shown in Figure 20 is dedicated to make a comparative study between the correctors PID, IMC and RST digital.

This interface has four oscilloscopes to visualize the comparative growth of control currents, valves at the turbine inlet, turbined water flow rates and frequency corrected output of the alternator.

Each corrector has a light that comes on when the corrected frequency is outside the normal operating range ([48, 52]). On the dashboard of our simulator we can visualize in real time the evolution of the power provided by the turboalternator (Pm) the load torque (Cr) and the engine torque (Cm) on the alternator shaft in the presence of the correctors PID, IMC and RST. The comparative growth of the frequencies corrected at the output of the alternator in time the real data presented by the simulator shows us that the one corrected by the RST corrector reveals a good accuracy and a satisfactory response speed.

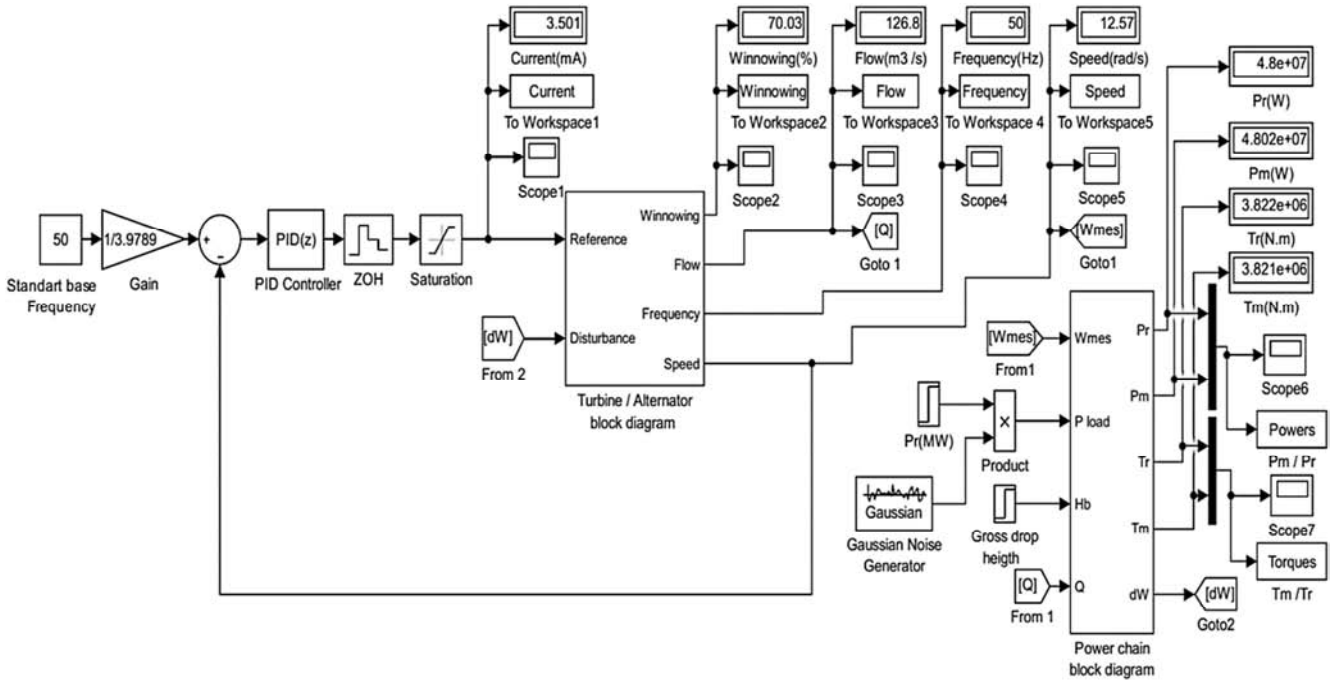

Figure 10. *Model of the Power Plant in the Presence of the PID Controller.*

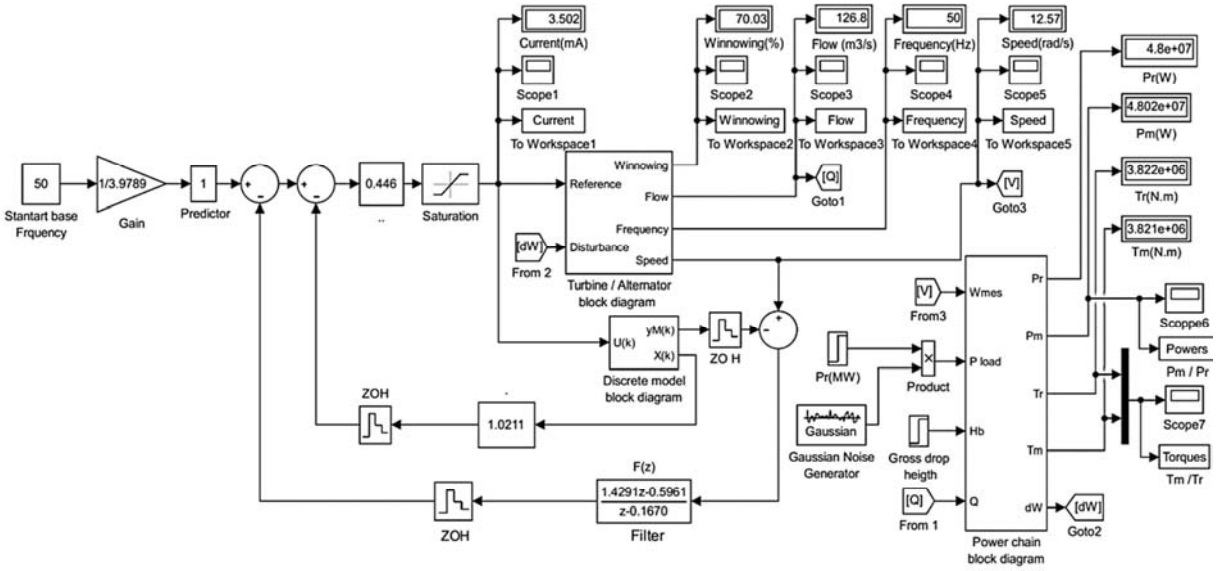

Figure 11. *Model of the Power Plant in the Presence of the IMC Controller.*

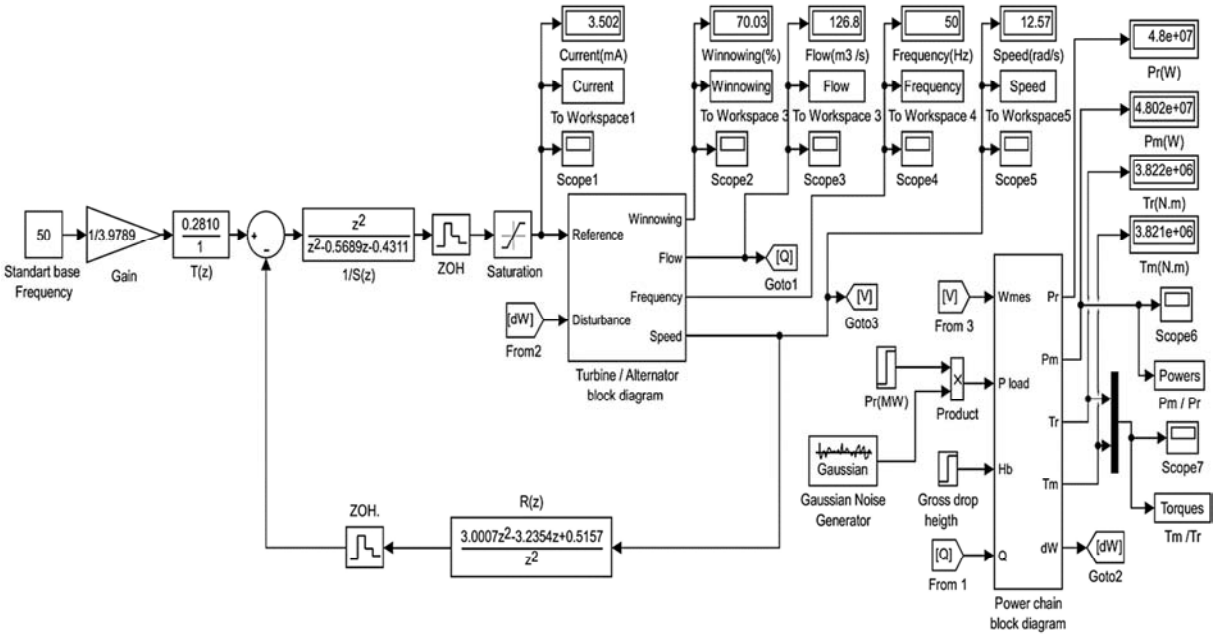

Figure 12. *Model of the Power Plant in the Presence of the RST Controller.*

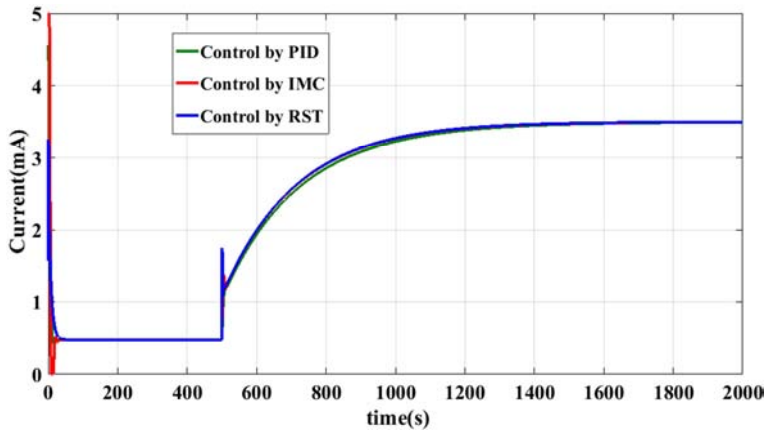

(a)

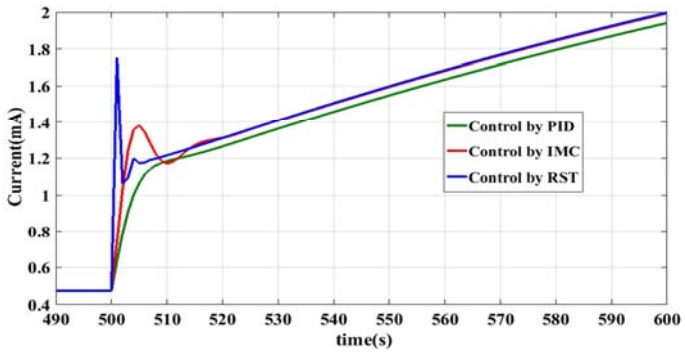

(b)

Figure 13. *Comparative Growth of the Control Currents of the Servomotor/Servo valve Assembly (a) and Comparative Growth of the Control Currents of the Servomotor/Servo valve Assembly zoom (b).*

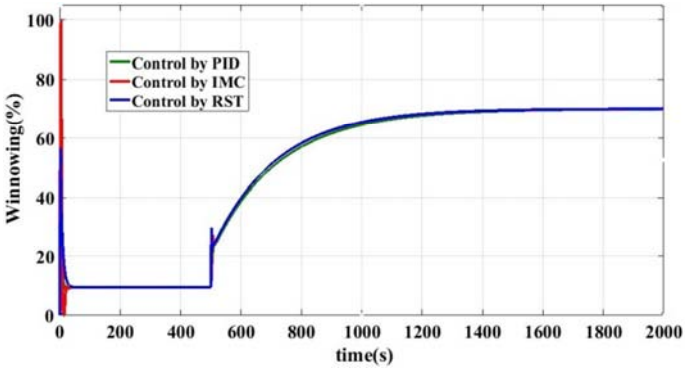

(a)

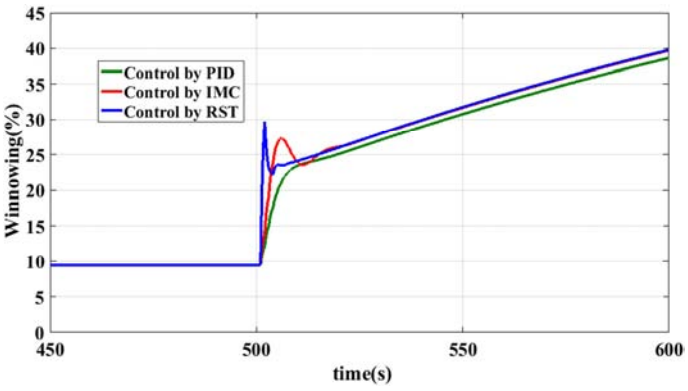

(b)

Figure 14. *Comparative Growth of the Valves at the Inlet of the Turbine (a) and Comparative Growth of the Valves at the Inlet of the Turbine zoom (b).*

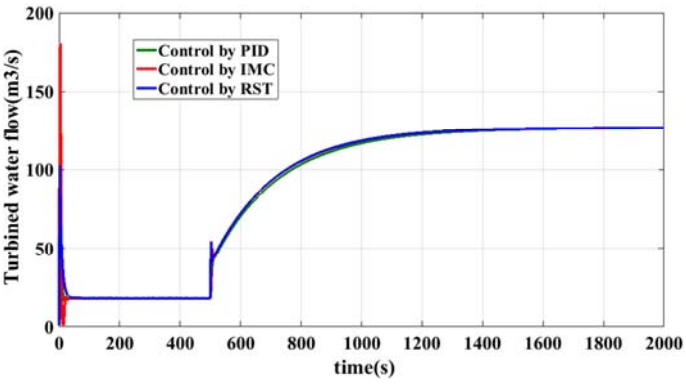

(a)

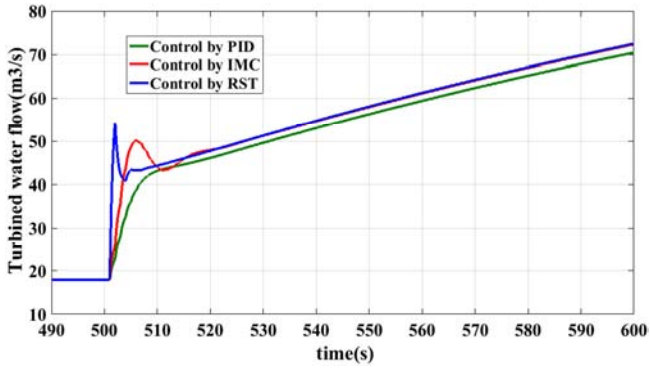

(b)

Figure 15. *Comparative Growth of Turbined Water Flow (a) and Comparative Growth of Turbined Water Flow zoom (b).*

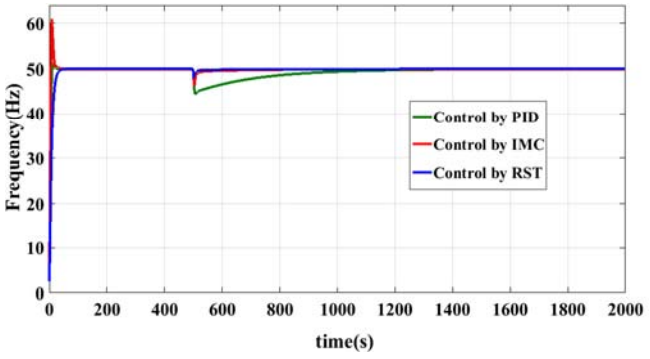

(a)

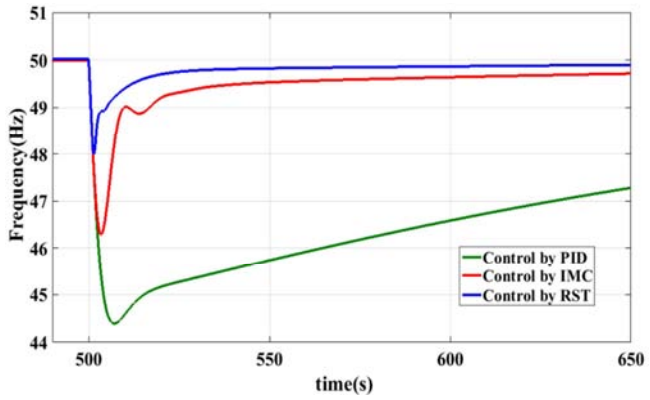

(b)

Figure 16. *Comparative Growth of Frequencies Corrected at the Output of the Alternator (a) and Comparative Growth of Frequencies Corrected at the Output of the Alternator zoom (b).*

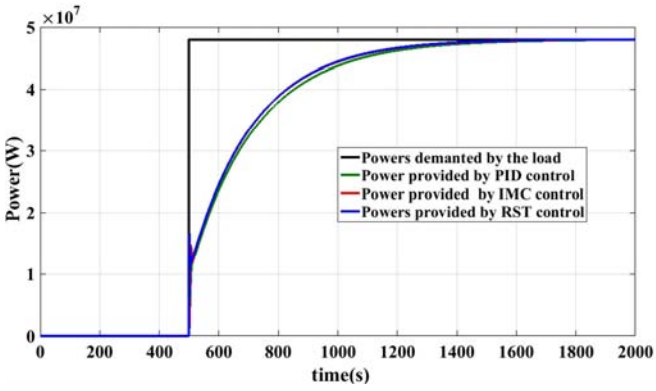

(a)

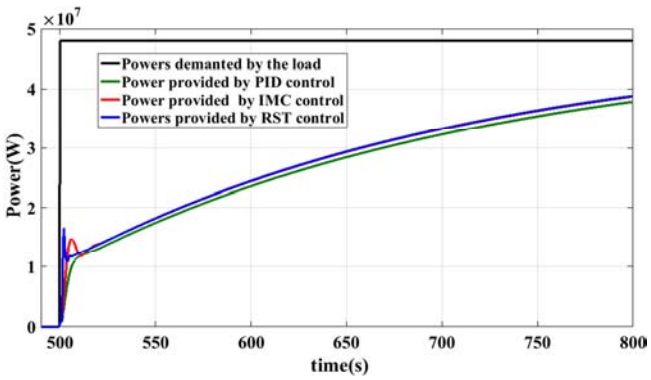

(b)

Figure 17. *Comparative Growth of the Powers Demanded by the Load and Powers Provided (a) and Comparative Growth of the Powers Demanded by the Load and Powers Provided zoom (b).*

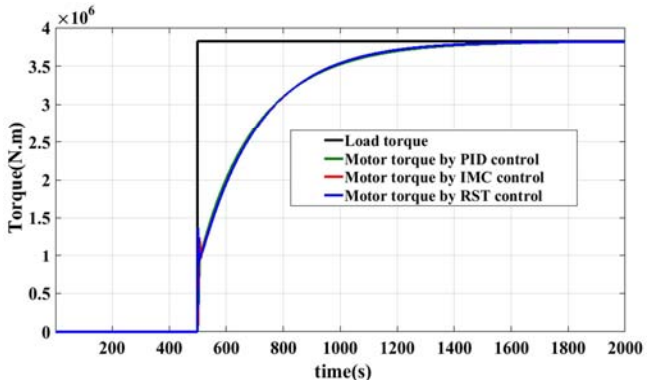

(a)

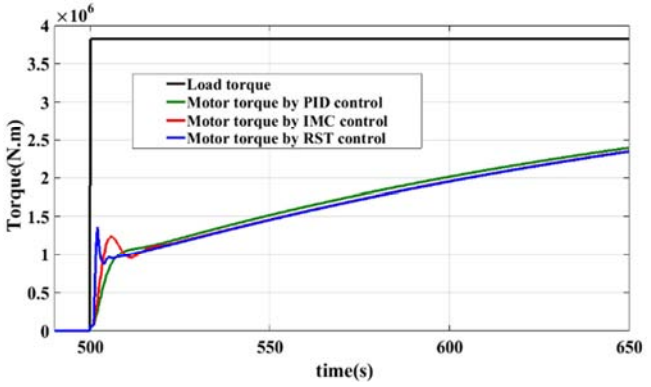

(b)

Figure 18. *Comparative Growth of Load Moments and Torques on the Alternator Shaft (a) and Comparative Growth of Load Moments and Torques on the Alternator Shaft zoom (b).*

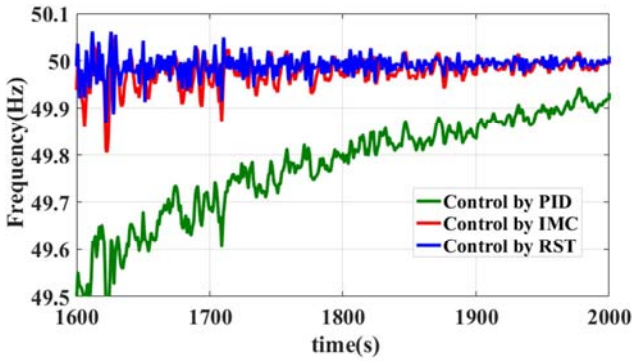

(a)

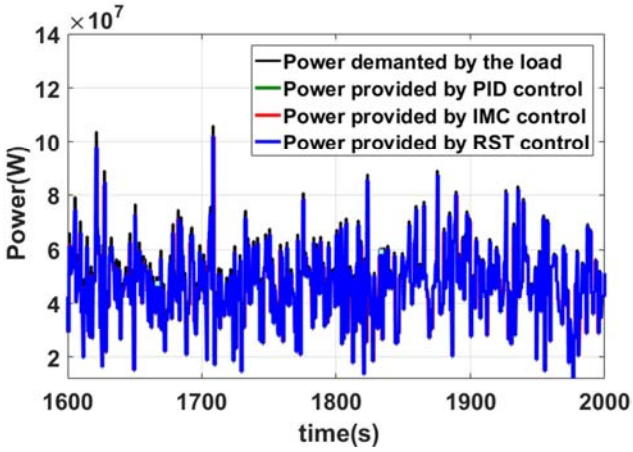

(b)

Figure 19. *Comparative Growth of Frequencies Corrected at the Output of the Alternator and Compared Growth of Powers Demanded by the Load and Powers Provided.*

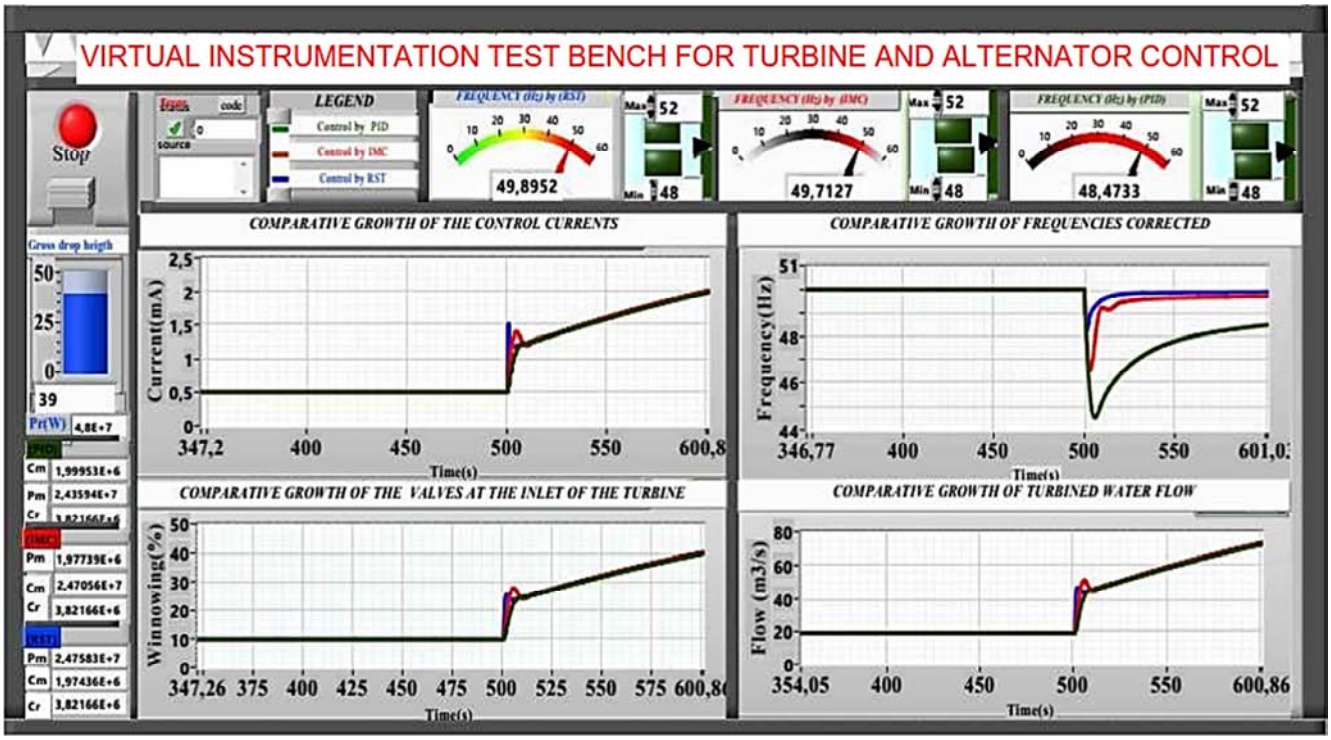

Figure 20. *Graphical Interface of the Virtual Test Bench for Turbine Control and Alternator (Digital PID control, Digital IMC and Digital RST).*

Table 2. *Comparisons of parameters of the hydroelectric power plant.*

Time (s)	Frequency (Hz)			Speed (rad/s)			Flow rate (m^3/s)		
	PID	IMC	RST	PID	IMC	RST	PID	IMC	RST
0	50,00	50,00	50,00	12,57	12,57	12,57	17,96	17,96	17,96
2	46,85	46,98	48,28	11,77	11,81	12,15	22,59	25,67	53,81
12	44,77	48,94	49,48	11,25	12,30	12,44	43,76	43,35	44,91
24	45,25	49,34	49,73	11,37	12,39	12,50	47,43	48,99	49,30
30	45,37	49,40	49,77	11,40	12,41	12,51	49,54	51,19	51,22
60	45,92	49,56	49,82	11,54	12,56	12,52	59,31	61,03	61,16
80	46,27	49,60	49,84	11,63	12,47	12,52	65,13	66,93	67,06
100	46,59	49,64	49,85	11,71	12,48	12,53	70,39	72,29	72,44
120	46,89	49,67	49,86	11,78	12,48	12,53	75,18	77,28	77,31
140	47,16	49,70	49,88	11,85	12,49	12,54	79,59	81,62	81,77

Time (s)	Frequency (Hz)			Speed (rad/s)			Flow rate (m^3/s)		
	PID	IMC	RST	PID	IMC	RST	PID	IMC	RST
160	47,40	49,73	49,89	11,91	12,50	12,54	87,24	85,67	85,82
250	48,27	49,82	49,93	12,13	12,52	12,55	97,65	99,83	99,97
350	48,90	49,89	49,95	12,29	12,54	12,55	108,0	109,9	110,1
700	49,76	49,98	49,99	12,51	12,56	12,56	122,8	123,5	121,6
900	49,90	49,99	50,00	12,54	12,56	12,57	125,2	125,5	125,6
1500	49,98	50,00	50,00	12,56	12,56	12,57	126,7	126,7	126,8

Table 2. *Continued.*

Time (s)	Winnowing (%)			Control current (mA)			Motor Torque (10^5N.m)			Power Produced (MW)		
	PID	IMC	RST	PID	IMC	RST	PID	IMC	RST	PID	IMC	RST
0	9,440	9,440	9,440	0,470	0,470	0,470	0,000	0,000	0,000	0,00	0,000	0,000
2	12,02	13,69	29,66	0,635	0,740	1,752	2,420	3,519	13,49	4,190	4,190	16,58
12	23,80	23,58	24,45	1,200	1,201	1,225	10,69	9,630	10,07	12,03	18,50	12,53
24	25,85	26,72	26,78	1,305	1,349	1,342	11,98	11,54	11,48	13,62	14,30	14,34
30	27,03	27,93	27,96	1,364	1,409	1,410	12,75	12,28	12,20	14,50	15,25	15,26
60	32,48	33,42	33,49	1,635	1,682	1,677	16,27	15,67	15,63	18,78	19,51	19,57
80	35,70	36,70	36,98	1,795	1,840	1,849	18,51	17,70	17,67	21,29	22,07	22,13
100	38,63	39,69	39,77	1,941	1,993	1,997	20,13	19,55	19,52	23,57	24,39	24,40
120	41,31	42,41	42,48	2,074	2,129	2,133	21,77	21,24	21,20	27,55	26,51	26,57
140	43,74	44,96	44,96	2,950	2,250	2,250	23,25	22,76	22,70	27,55	28,44	28,50
160	45,97	47,21	47,21	2,305	2,362	2,362	24,58	24,15	24,15	29,90	30,10	30,25
250	53,83	55,09	55,09	2,696	2,755	2,759	29,18	29,01	29,00	35,41	36,33	36,30
350	59,54	60,63	60,70	2,981	3,030	3,038	32,44	32,46	32,40	39,80	40,70	40,75
700	67,73	68,21	68,24	3,387	3,411	3,412	36,96	37,10	37,10	46,22	46,60	46,20
900	69,06	69,32	69,33	3,453	4,460	3,467	37,69	37,70	37,78	47,26	47,40	47,47
1500	69,96	70,00	70,00	3,498	3,500	3,600	38,18	38,20	38,22	47,97	48,00	48,00

7. Conclusion

The aim of this work was to implement new types of robust correctors in order to increase the efficiency of the speed control system of a group of the Songloulou hydroelectric power plant. The results of simulating the three types of controllers applied to the Songloulou hydroelectric power plant model in a disturbing environment corroborated our predictions that a robust controller (in this case RST) would be more appropriate for increasing the efficiency of the control system of frequency at the output of the alternator. It would be interesting to implement the RST corrector on the control chart of the turbine speed control system in real size hydroelectric plants.

References

[1] P. Podrzaj, M. Miklavcic and A. Bergant. ‘‘Hydro Power Plant Simulator for Control Algorithm Testing’’. In: International Electrotechnical And Computer Science Conference (2014), pp. 136–4.

[2] IEEE Committee Report, Hydraulic Turbine and Turbine Control Models for System Dynamic Studies, IEEE Transaction on Power Systems, vol. 7, no. 1, pp. 167-179, Febuary 1992.

[3] Kundur P., Power System Stability and Control, Mc Graw Hill, 1994.

[4] Hannet L. N., Fardanesh B., Field test to validate hydroturbine-governor model structure and parameters, IEEE Transaction on Power Systems, vol. 9, 1994, pp. 1744-1751.

[5] Arnaurovic D. B., Skataric D. M, Suboptimal design of Hydroturbinegovernors, IEEE Transactionsonenergy Conversion, Vol. 6/3, 1991.

[6] Jean Ricard. Equipement thermique des usines génératrices d’énergie électrique. Troisièmeédition. Dunod, Paris, 1962.

[7] S. Boyd and C. Barrat. Linear Controller Design: Limits of Performance. Prentice Hall, 1991.

[8] E. Laroche, Y. Bonnassieux, H. Abou-Kandil, and J. Louis. Controller design and robustness analysis for induction machine-based positioning system. Control Engineering Practice, 12 (6):757–767, June 2004.

[9] LE Hoang Bao, "Contribution aux méthodes de synthèse de correcteurs d’ordres réduits sous contraintes de robustesse et aux méthodes de réduction de modèles pour la synthèse robuste en boucle fermée". PhD thesis. Institut National Polytechnique de Grenoble - INPG, 2010.

[10] Gilberto Gonzalez and Octavio Barriga. A Hydroelectric Plant connected to Electrical Power System: A Bond Graph Approach, Recent Advances in Technologies, Maurizio AStrangio (Ed.), ISBN: 978- 953-307-017-9 (2009).

[11] A. Yeremou Tamtsia, J. M. Nyobe Yome, G. M. Ngaleu, J. C. Ndzana. Contrôle de la fréquence dans une centrale de production d’énergie électrique. Sciences, Technologies et Développement, Edition spéciale, ISSN 1029 – 2225 - e - ISSN 2313 – 6278, pp 39-44, Juillet 2016.

[12] Peter Breedveld. Bond Graphs. Encyclopedia Life Support Systems contribution- preliminary version knowledge Foundations AREA. THEME 6.43. Control System; Robotics and Automation Topic 6.43.7 Modeling and Simulation.

[13] Gilbert Riollet, Théorie générale des turbomachines. Techniques de l'Ingénieur, traité Génie mécanique.

[14] Mohamed Tafraouti. Contribution à la commande de systèmes électrohydrauliques: PhD thesis. Université Henry poincaré-Nancy I, 2006.

[15] Centrale de Songloulou, turbines et régulateurs, manuel d'entretien.

[16] G. Franklin, J. Powell, and L. Workman, Digital control of dynamic systems. Addison Wesley, Wokingham, 1989.

[17] C. I. Huang, "Computer Aided Design of Digital Controllers," M. S. thesis, Auburn University, Auburn, AL, 1981.

[18] M. Chakib, A. Essadki, T. Nasser. A Comparative Study of PI, RST and ADRC Control Strategies of a Doubly Fed Induction Generator Based Wind Energy Conversion System. International Journal of Renewable Energy Research. Vol.8, No.2, June, 2018. pp 967-973.

[19] P. Ostalczyk, Variable-, Fractional-Order RST/PID Controller Transient Characteristics Calculation. IEEE, 23rd International Conference on Methods & Models in Automation & Robotics (MMAR), 2018. pp 93-98.